Investigation of Dynamic Properties of a Novel Capacitive-based Sensing Skin for Nondestructive Testing

by Hussam Saleem*, Austin Downey†, Simon Laflamme‡, Matthias Kollosche§, and Filippo Ubertini¶

ABSTRACT

A capacitive-based soft elastomeric strain sensor was recently developed by the authors for structural health monitoring applications. Arranged in a network configuration, the sensor becomes a sensing skin, where local deformations can be monitored over a global area. The sensor transduces a change in geometry into a measurable change in capacitance, which can be converted into strain using a previously developed electromechanical model. Prior studies have demonstrated limitations of this electromechanical model for dynamic excitations beyond 15 Hz, because of a loss in linearity in the sensor's response. In this paper, the dynamic behavior beyond 15 Hz is further studied, and a new version of the electromechanical model is proposed to accommodate dynamic strain measurements up to 40 Hz. This behavior is characterized by subjecting the sensor to a frequency sweep and identifying possible sources of nonlinearities beyond 15 Hz. Results show possible frequency dependence of the materials' Poisson's ratios, which are successfully modeled and integrated into the electromechanical model. This demonstrates that the proposed sensor can be used for monitoring and evaluation of structural responses up to 40 Hz, a range covering the vast majority of the dominating frequency responses of civil infrastructures.

KEYWORDS: nondestructive testing, structural health monitoring, soft elastomeric capacitor, capacitive sensor, vibration monitoring, sensing skin.

Introduction

Structural health monitoring (SHM) is defined as the automation of nondestructive testing (NDT), aimed at diagnosing, localizing, and prognosing structural damages to ensure public safety and structural integrity (Harms et al., 2010). A particular challenge in SHM is associated with the magnitude of the geometries under assessment (Laflamme et al., 2015). Existing sensing solutions are typically difficult to scale up to this mesoscale, because of technical and economic constraints. These include limitations in data interpretation, cost of installation, and scalability of the transducers (Farrar and Lieven, 2007; Laflamme et al., 2013a).

Recent advances in conductive polymers have enabled the development of scalable sensors. Their measurement principles are typically based on monitoring local states over global areas by deploying large arrays of flexible sensing substrates, analogous to sensing skins. For instance, a few prior studies investigated carbon nanotube-based flexible strain sensors, and others proposed to utilize flexible sensing sheets of strain gages (Hu et al., 2014; Kang et al., 2006; Loh et al., 2009; Srivastava et al., 2011; Tung et al., 2014).

The authors recently proposed a highly scalable sensing skin for measurement of strain onto mesosurfaces (Laflamme et al., 2013a). The skin is composed of a dense network of soft elastomeric capacitors (SECs). The dielectric of an SEC is fabricated from a styrene-co-ethylene-co-butylene-co-styrene (SEBS)

---

* Ph.D. candidate, M.S., Department of Civil, Construction, and Environmental Engineering, Iowa State University, Ames, Iowa.

† Ph.D. candidate, M.S., Department of Civil, Construction, and Environmental Engineering, Iowa State University, Ames, Iowa.

‡ Ph.D., Department of Civil, Construction, and Environmental Engineering, Department of Electrical and Computer Engineering, Iowa State University, Ames, Iowa.

§ Ph.D., Institute of Physics and Astronomy, Potsdam University, Potsdam, Germany.

¶ Ph.D., Department of Civil and Environmental Engineering, University of Perugia, Perugia, Italy.

polymer matrix doped with titanium dioxide (TiO_2) nanoparticles, and the electrodes are constituted also from SEBS but are doped with carbon black particles. The SEC transduces a change in its geometry into a measurable change in its capacitance. Other capacitive-based sensors have been proposed in literature for applications to humidity, pressure, strain, and triaxial measurements (Arshak et al., 2000; Dobrzynska and Gijs, 2013; Hong et al., 2012; Lipomi et al., 2011; Suster et al., 2006). The proposed SEC differs from other sensors by being inexpensive and easy to fabricate, thus being highly scalable.

The utilization of the SEC technology for NDT has been demonstrated, including applications to fatigue crack detection, surface strain measurements, and extraction of deflection shapes (Kharroub et al., 2015; Laflamme et al., 2013b; Wu et al., 2015). These applications were focused on static and quasi-static behaviors. Recent investigations have been conducted on the characterization of the dynamic behavior of the SEC, with applications to monitoring vibration signatures (Laflamme et al., 2015; Ubertini et al., 2014). Both studies concluded that, while the sensor can detect a change in dynamic properties, it provides only a linear response for mechanical excitations up to 15 Hz.

This paper investigates the dynamic response of the SEC over a wider range of excitation, considering mechanical frequencies up to 40 Hz, which covers a wide range of structural dynamics found in mesosystems. Note that unless noted otherwise, the term "frequency" in this paper refers to a mechanical frequency, not electrical. The electrical frequency-dependence of SEBS filled with TiO_2 has been thoroughly discussed in literature (Kollosche et al., 2011; Stoyanov et al., 2010). The objective of this paper is to develop an augmented electromechanical model that accommodates for possible sources of nonlinearity beyond 15 Hz, to enable SHM applications up to 40 Hz, a range covering the vast majority of the dominating frequency responses of civil infrastructures.

It was hypothesized that a possible source of nonlinearity arises from a non-negligible frequency-dependence of the SEBS's Poisson's ratio due to its viscoelasticity (Kugler et al., 1990; Pritz, 2007; Tshoegl et al., 2002; Wada et al., 1962). A laboratory-based study was conducted to test the hypothesis by investigating the change in the sensor's sensitivity as a function of frequency. Its dynamic behavior was characterized up to 40 Hz based on the assumption that this sensitivity is purely explained by the frequency-dependence of the Poisson's ratio. This model was used to develop an augmented electromechanical model for the SEC.

The rest of the paper is organized as follows. The second section presents the background on the technology, which includes the fabrication technique and the original electromechanical model. The third section investigates the sensor's dynamic behavior, and develops an augmented electromechanical model that covers excitations up to 40 Hz. The final section concludes the paper.

Background

This section provides a background on the SEC technology. It includes a description of the fabrication process and a derivation of the original electromechanical model.

Fabrication Technique

The fabrication process of an SEC is described in detail in an outside work (Kharroub et al., 2015). Briefly, SEBS is dissolved in toluene, and the solution is mixed with 15 vol% TiO_2 to increase permittivity and durability of the polymer. Uniform dispersion of the nanoparticles is obtained via sonication using a sonic dismembrator for 10 min. The sonicated solution is then casted on an 80 × 80 mm non-stick glass plate and left overnight for the solvent to evaporate, which creates the dielectric. Meanwhile, 10 vol% carbon black is added to another SEBS-toluene solution and dispersed in a sonic bath for 6 h. The resulting conductive paint is applied to the top and bottom surfaces of the dielectric to create electrodes. Copper tape is embedded in the wet conductive paint, on each side of the dielectric, to enable mechanical connections to the data acquisition system (DAQ). Figure 1a shows a picture of the resulting SEC.

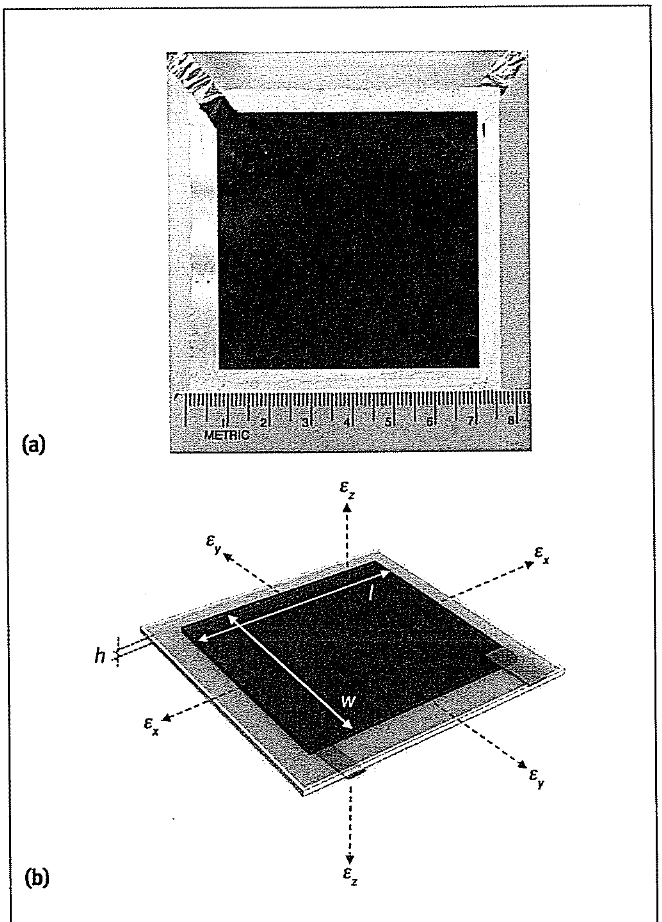

Figure 1. Soft elastomeric capacitor: (a) picture (75 × 75 mm^2); and (b) reference axis.

Electromechanical Model

The SEC is designed to measure in-plane strain along the X-Y plane shown in Figure 1b. Assuming low electrical frequency measurements (< 1 kHz), the SEC can be simplified as a non-lossy parallel plate capacitor with capacitance, C:

$$C = e_0 e_r \frac{A}{h} \tag{1}$$

where

$e_0 = 8.854$ pF/m is the vacuum permittivity,
e_r is the polymer relative permittivity,
$A = w \times l$ is the area of the sensor electrodes of width w and length l,
h is the thickness of the dielectric.

Assuming small strain, one can take the differential of Equation 1 to obtain an expression for the change in capacitance ΔC:

$$\frac{\Delta C}{C} = \left(\frac{\Delta l}{l} + \frac{\Delta w}{w} - \frac{\Delta h}{h}\right) = \varepsilon_x + \varepsilon_y - \varepsilon_z \tag{2}$$

where

ε_x, ε_y, and ε_z are strains in the X, Y, and Z directions as shown in Figure 1b.

An expression relating ε_z to ε_x and ε_y can be obtained using Hooke's law for plane stress conditions.

$$\varepsilon_z = -\frac{v}{1-v}\left(\varepsilon_x + \varepsilon_y\right) \tag{3}$$

The final form of the electromechanical model is obtained by integrating Equation 3 in Equation 2:

$$\frac{\Delta C}{C} = \lambda\left(\varepsilon_x + \varepsilon_y\right) \tag{4}$$

where

$$\lambda = \frac{1}{1-v} \tag{5}$$

is the gage factor.

For SEBS, $v \approx 0.49$, which yields a gage factor $\lambda \approx 2$ (Wilkinson et al., 2004).

Investigation of Dynamic Behavior

In this section, the behavior of the SEC is investigated in the frequency (f) range 1 to 40 Hz. Response linearity and sensitivity as a function of a frequency-dependent Poisson's ratio are studied. Finally, an augmented electromechanical model where v is allowed to be frequency-dependent in Equation 12 is presented.

Methodology

The test setup is shown in Figure 2a. It consists of an aluminum plate of dimensions $432 \times 102 \times 0.68$ mm^3 excited axially, onto which an SEC is adhered. Two resistive strain gages (RSGs) were installed onto the back of the plate opposite to the SEC, measuring strain in both the X and Y directions independently, where X denotes the direction of the applied load and Y is transverse to the load and in-plane with the SEC. Data from the SEC were recorded using an off-the-shelf DAQ at a sampling rate of 250 Hz.

The axial excitation was provided by a servo-hydraulic testing machine and consisted of a time-varying harmonic tensile force sweeping from 1 to 40 Hz in 1 Hz increments. The strain time history is shown in Figure 2b. Because of equipment limitations, the displacement decreased with increasing frequency, as observed in Figure 2b.

Parameters of interest in the study of the dynamic behavior of the SEC are the linearity of the response and the

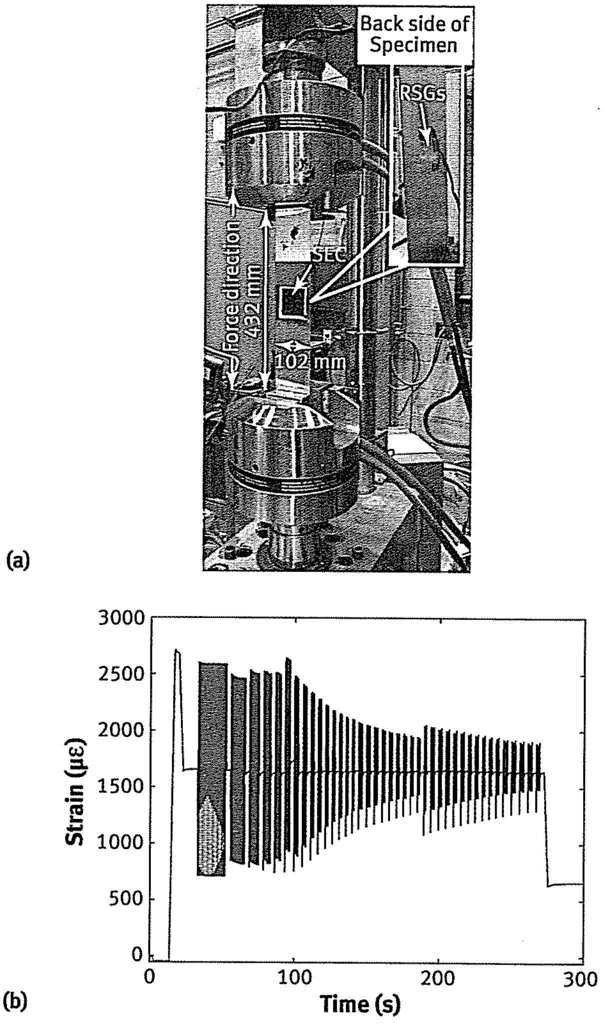

Figure 2. Soft elastomeric capacitor (SEC) test: (a) experimental setup; and (b) resistive strain gage (RSG) strain data.

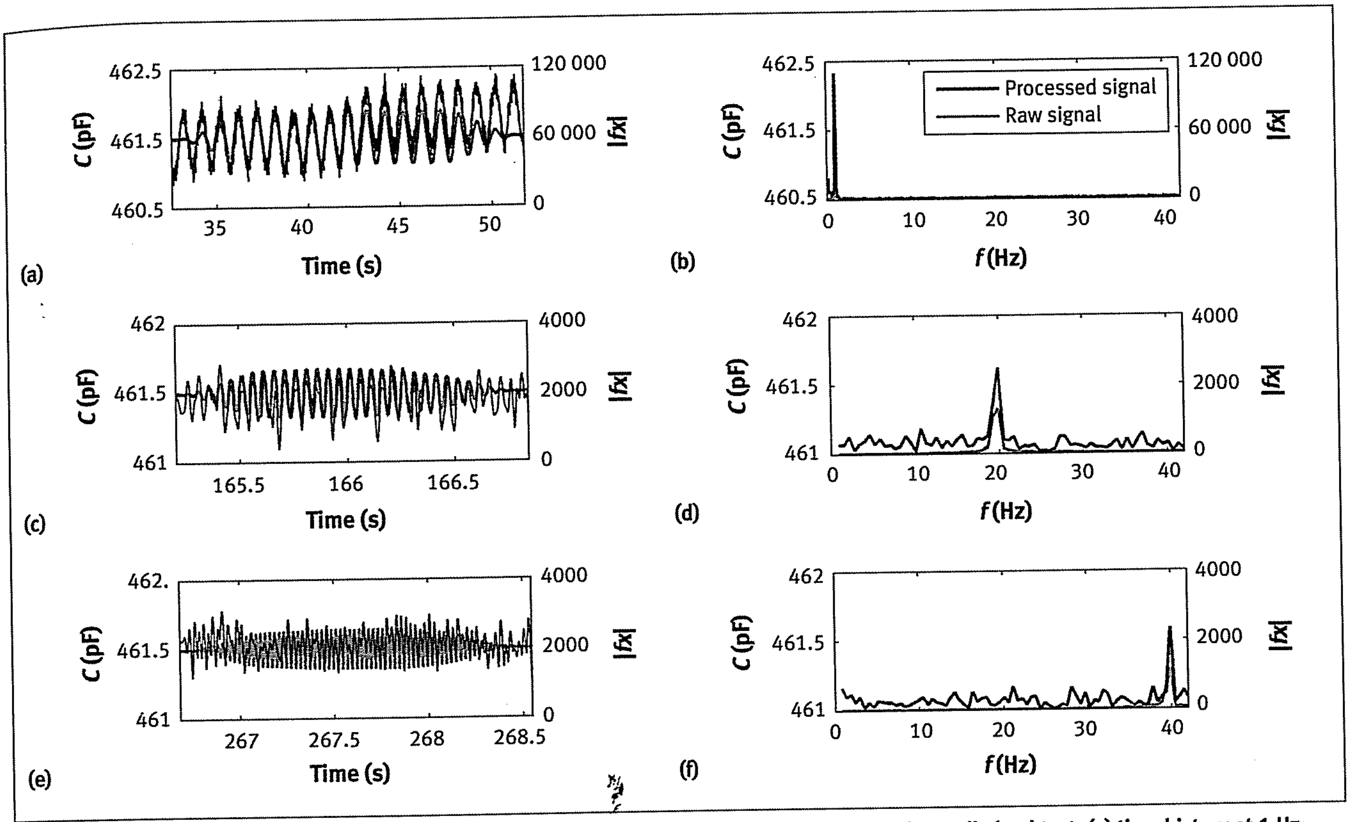

Figure 3. Signals provided by resistive strain gages and soft elastomeric capacitor in the harmonic tensile load test: (a) time history at 1 Hz; (b) fourier transform at 1 Hz; (c) time history at 20 Hz; (d) fourier transform at 20 Hz; (e) time history at 40 Hz; and (f) fourier transform at 40 Hz.

gage factor as a function of the excitation frequency. For each frequency of interest, the time histories of both the load input and the sensor's capacitance output were extracted using a window function. A band-pass filter designed around this frequency was applied to both time series (input and output) to reduce noise. The linearity was assessed by plotting the filtered output versus the filtered input, and the experimental gage factor was back-calculated from Equation 11 using the measured ε_x and ε_y from the resistive strain gages and ΔC.

Figure 3 shows the filtered time series following this methodology at three particular frequencies: 1, 20, and 40 Hz, which represent the lowest, middle, and highest frequencies in the sweep. A salient feature in the plots is the increase in the level of noise with the increase in frequency. This can be attributed to electromagnetic interference, despite careful attention to minimize such noise in the experimental setup (for example, by utilizing shielded cables and grounding of components).

Figure 4 shows the wavelet transform of the raw signal (Figure 4a) compared against the processed signal (Figure 4b), using morlet wavelets. The wavelet transform is normalized at each discrete time interval to the highest wavelet amplitude. The black line is the input frequency content. Results validate the signal processing methodology and show good agreement between the dynamic input and sensor output across the entire frequency range from 1 to 40 Hz.

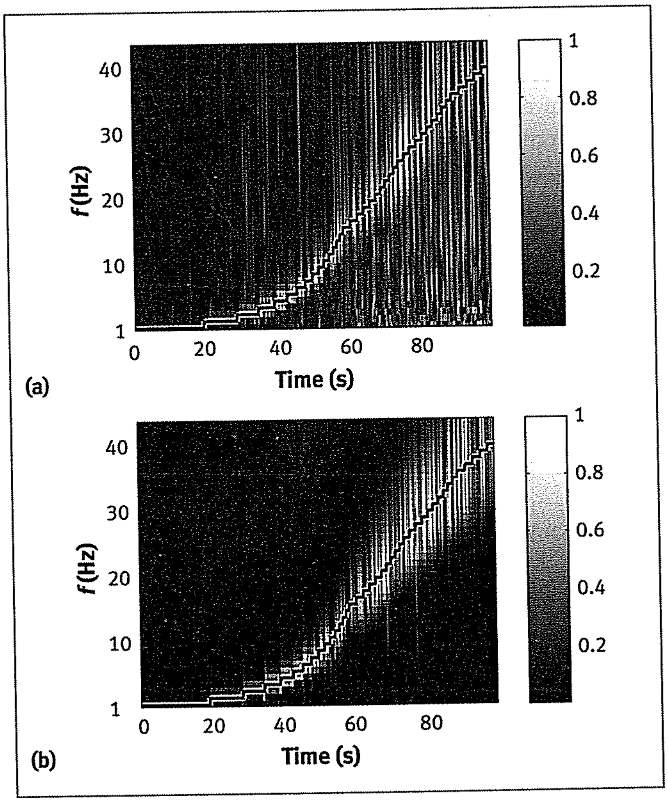

Figure 4. Wavelet transform of the: (a) raw data; and (b) processed data.

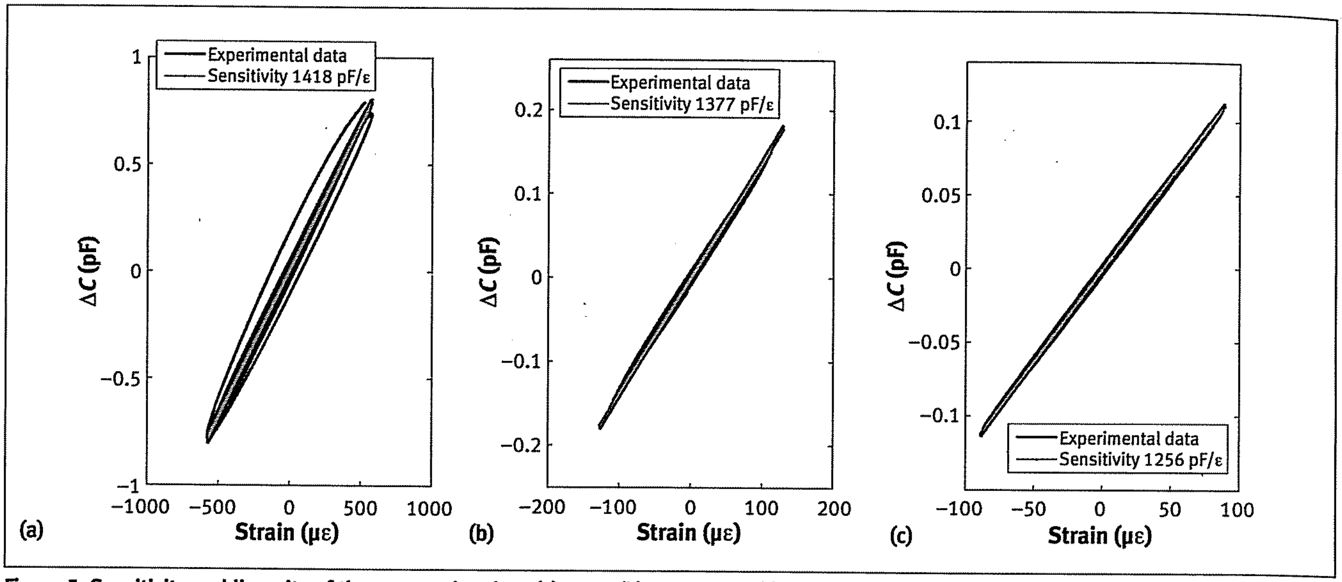

Figure 5. Sensitivity and linearity of the sensor signal at: (a) 1 Hz; (b) 20 Hz; and (c) 40 Hz.

Results

The sensor linearity and sensitivity were studied through the investigation of the sensor's response as a function of frequencies. Figure 5 shows plots of the response of the SEC against the measured additive strain $\varepsilon_x + \varepsilon_y$. The red line is the linear fit obtained via linear regression. The quality of the linear fit represents the linearity of the sensor, while the slope of the regression represents its sensitivity, $S = \Delta C / (\varepsilon_x + \varepsilon_y)$. The root mean square error (RMSE) was used as a performance measure for linearity, plotted in Figure 6. The figure shows higher error at lower frequency excitations. This could be attributed to the higher magnitude of the strain input at lower frequencies. Yet, the overall RMSE shows a good linearity of the sensor.

Results from Figure 5 show a decrease in sensitivity with increasing frequency. This can also be observed in the plotted gage factor, calculated from the experimental results, shown in Figure 7. A two-term power series provided the best fit of the experimental gage factor data. This fit illustrates the apparent reduction in the gage factor as the frequency increases. The sensitivity, S, was reduced by 2.9% at 20 Hz and 11.5% at 40 Hz with respect to the reference, S, at 1 Hz as shown in Figures 5a, 5b, and 5c respectively.

As explained in the introduction, the change in the sensor's sensitivity was modeled assuming that it could be explained by the complex Poisson's ratio of the material. Consider the strain modeled as a complex component:

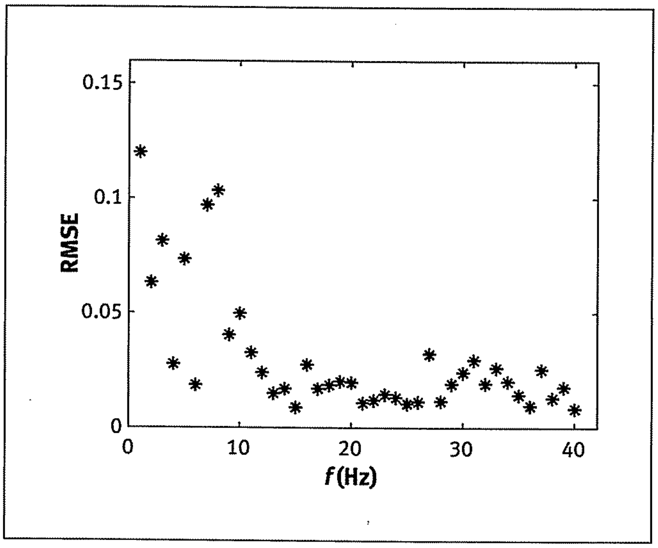

Figure 6. Root mean square error (RMSE) fitting for the capacitance data.

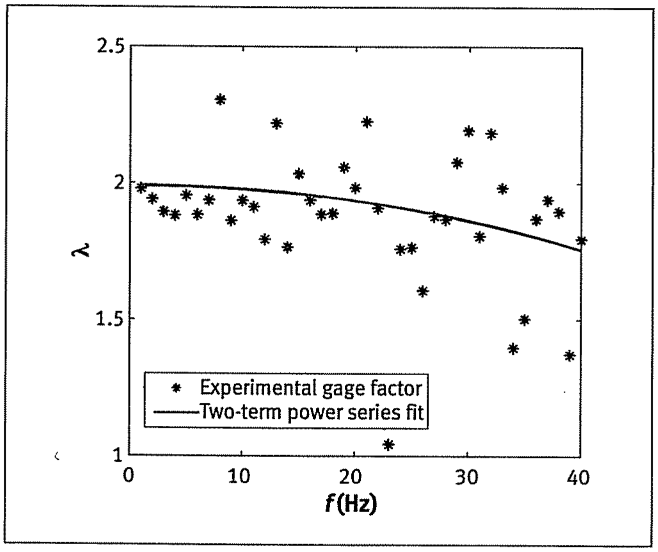

Figure 7. Experimental gage factor.

(6) $$\varepsilon_x(t) = \hat{\varepsilon}_x e^{j\omega t}$$
$$\varepsilon_y(t) = \hat{\varepsilon}_y e^{j\omega(t-\Delta t)} = \hat{\varepsilon}_y e^{j(\omega t - \delta_v)}$$

where
- t is the time,
- $\hat{\varepsilon}_x$ is the amplitude of the axial strain,
- $\hat{\varepsilon}_y$ is the amplitude of the lateral strain modeled with the same frequency response as $\hat{\varepsilon}_x$, but with a phase lag $\delta_v = \omega \Delta t$, $\omega = 2\pi f$ (Pritz, 2007).

The complex Poisson's ratio is the ratio of the lateral to the axial strains:

(7) $$\bar{v}(j\omega) = \frac{\varepsilon_y(t)}{\varepsilon_x(t)} = \frac{\hat{\varepsilon}_y}{\hat{\varepsilon}_x} e^{-j\delta_v} = \frac{\hat{\varepsilon}_y}{\hat{\varepsilon}_x}(\cos\delta_v - j\sin\delta_v)$$
$$= v_d(\omega) - jv_l(\omega) = v_d(\omega)(1 - j\eta_v[\omega])$$

where
- ν_d is the dynamic Poisson's ratio,
- ν_l is the loss component,
- η_v is the Poisson's loss factor.

(8) $$\eta_v(\omega) = \frac{v_l(\omega)}{v_d(\omega)}$$

The absolute value of $\bar{v}(j\omega)$ (Equation 7) provides an expression that relates ν_d and η_v to the magnitude of the Poisson's ratio $|\bar{v}(j\omega)|$:

(9) $$|\bar{v}(j\omega)| = \frac{\hat{\varepsilon}_y}{\hat{\varepsilon}_x} = \sqrt{(v_d^2 + v_l^2)} = v_d\sqrt{(1+\eta_v^2)}$$

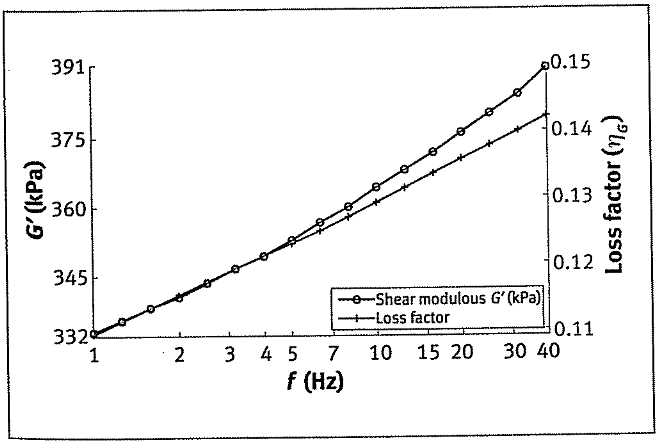

Figure 8. Storage moduli (G') and loss factor (η_G) as functions of frequency for the soft elastomeric capacitor (styrene-co-ethylene-co-butylene-co-styrene + titanium dioxide).

Further, it was shown in an outside work that, assuming an incompressible material ($\nu_d \approx 0.5$), the Poisson's loss factor relates to the material's shear loss modulus, η_G, through the following expression (Pritz, 2007).

(10) $$\frac{\eta_v(\omega)}{\eta_G(\omega)} \approx 1 - 2v_d(\omega)$$

A set of experimental values was obtained for η_G by conducting a dynamic mechanical analysis (DMA) of the studied material. Figure 8 presents the results. Measurements indicate an increase in the real part of the shear modulus, G', and the shear loss modulus, $\eta_G = G''/G'$, with increasing frequency. This phenomenon can be attributed to the polymer-particles and particle-particle interactions (Fröhlich et al., 2005).

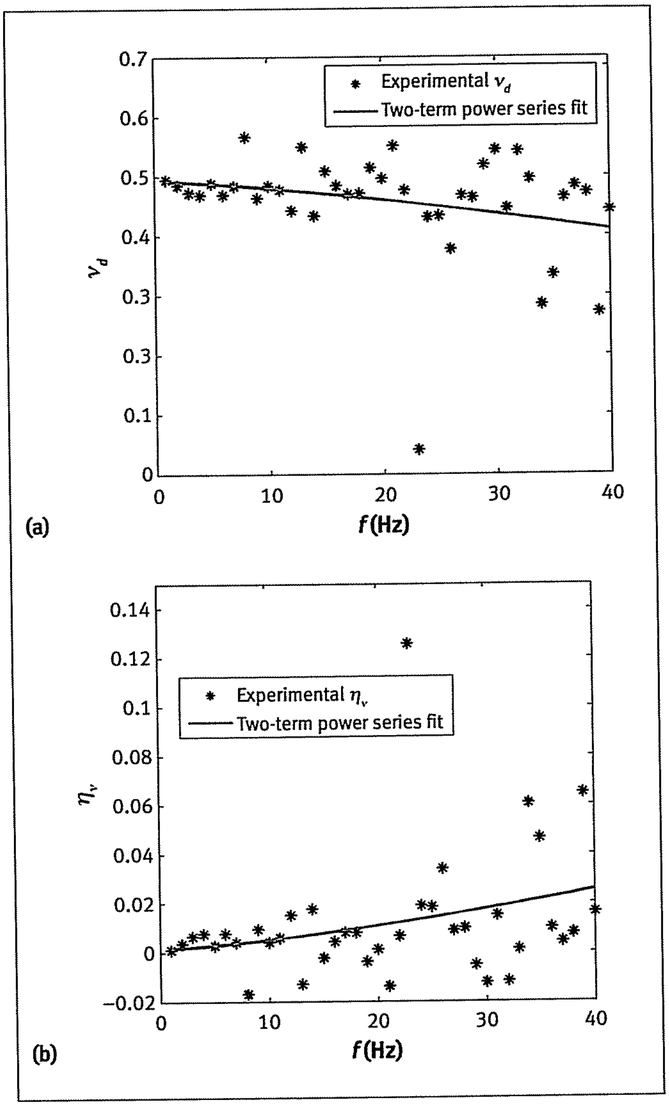

Figure 9. Results obtained over frequency range 1–40 Hz: (a) dynamic Poisson's ratio; and b) Poisson's ratio loss factor plotted against frequency.

Values for η_G obtained from the DMA, combined with the experimental Poisson's ratio coefficients derived from S and Equation 12, can be used with Equations 9 and 10 to find ν_d and η_ν. Figures 9a and 9b show the results obtained over the frequency range of 1 to 40 Hz. Results show a decreasing dynamic Poisson's ratio, ν_d, and an increasing Poisson's loss factor, η_ν, with increasing frequency. The red solid line is the data fit using a two-term power series fit. This fit can be used to characterize the changes in ν_d and η_ν as a function of ω, and yield mathematical expressions to generate the adjusted electromechanical model.

Adjusted Electromechanical Model

Using results from the previous section, an adjusted electromechanical model can be generated that accounts for the change in the material's behavior as the frequency increases. The proposed model is a variation of Equation 11:

$$\frac{\Delta C}{C} = \lambda_{\text{adj}}\left(\varepsilon_x + \varepsilon_y\right) \tag{11}$$

where

$$\lambda_{\text{adj}} = \frac{1}{1 - \upsilon_{\text{adj}}} \tag{12}$$

and

$$\upsilon_{\text{adj}}(\omega) = \upsilon_d(\omega)\sqrt{1 + \eta_\upsilon^2(\omega)} \tag{13}$$

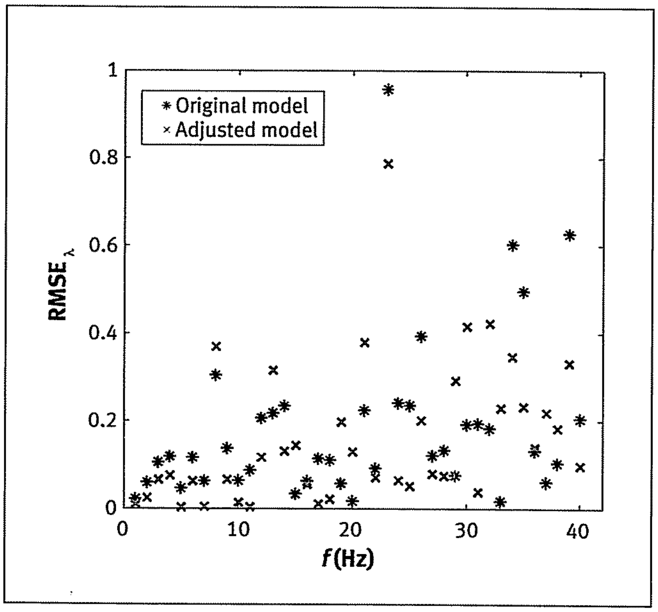

Figure 10. Root mean square error (RMSE) on the estimation of λ as a function of frequency.

where

the expressions for ν_d and η_ν are directly obtained from the investigation in the previous section:

$$\begin{aligned} \upsilon_d(\omega) &= -4.65 \times 10^{-5}\omega^{1.35} + 0.49 \\ \eta_\upsilon(\omega) &= 1.27 \times 10^{-5}\omega^{1.36} + 0.0016 \end{aligned} \tag{14}$$

where

the adjusted electromechanical model is valid up to 40 Hz.

Figure 10 shows the RMSE on the estimation of λ as a function of frequency, for both the original and adjusted models. Table 1 summarizes the results for frequency ranges of interest. Results show that the adjusted model provides an overall improvement on the estimation of RMSE$_\lambda$ by 14.3% over the range of 1 to 40 Hz. The vast majority of this improvement is from the estimation in the 16 to 40 Hz range, where the adjusted model improves the estimation on RMSE$_\lambda$ by 15.8%. This demonstrates the superiority of the new model over the original model. Note that the RMSE$_\lambda$ over the range of 1 to 15 Hz is only marginally improved, which demonstrates the validity of the original model over the 1 to 15 Hz range.

TABLE 1
Root mean square error of λ

Range	Original model	Adjusted model	Improvement
1 to 40 Hz	0.266	0.228	14.3%
1 to 15 Hz	0.146	0.143	2.1%
16 to 40 Hz	0.317	0.267	15.8%

Conclusion

This paper presented a novel sensor for NDT. The sensor is an SEC. Arranged in a network configuration, it is analogous to sensing skin, in the sense that it can measure discrete changes over a global area. Previous work on the SEC developed an electromechanical model, which showed to be valid for excitations up to 15 Hz. Here, adjusting the electromechanical model was proposed to cover a broader range of excitations, up to 40 Hz.

It was hypothesized that a possible source of nonlinearities arose from a non-negligible frequency-dependence of the SEBS's Poisson's ratio due to its viscoelasticity. An empirical study of the SEC's material response as a function of frequency was conducted. Results show that the experimental Poisson's ratio decreased with increasing mechanical frequency. This relationship was successfully modeled as a complex Poisson's ratio, and led to an adjusted electromechanical model that could account for the sensor's nonlinearities up to 40 Hz. Note that while it is possible that the nonlinearities come from other sources, this model can still be used to transduce changes in capacitance into strain.

By covering an excitation range up to 40 Hz, the adjusted electromechanical model enables measurements over a frequency range that covers the vast majority of dynamic responses in civil structures. It empowers the SEC technologies with dynamic measurement capabilities, useful for vibration-based SHM and NDT.

ACKNOWLEDGMENTS

The work presented in this paper is partially funded by a Fellowship Award from the American Society for Nondestructive Testing. The development of the soft elastomeric capacitor technology is supported by grant no. 1001062565 from the Iowa Alliance for Wind Innovation and Novel Development and grant no. 13-02 from the Iowa Energy Center. This work is also partially funded under U.S. National Science Foundation grant no. 4782025, which supports the activities of the Integrative Graduate Education and Research Traineeship in Wind Energy Science, Engineering, and Policy at Iowa State University.

REFERENCES

Arshak, K.I., D. McDonagh, and M.A. Durcan, "Development of New Capacitive Strain Sensors Based on Thick Film Polymer and Cermet Technologies," *Sensors and Actuators A: Physical*, Vol. 79, No. 2, 2000, pp. 102–114.

Dobrzynska, J.A., and M.A.M. Gijs, "Polymer-based Flexible Capacitive Sensor for Three-axial Force Measurements," *Journal of Micromechanics and Microengineering*, Vol. 23, No. 1, 2013.

Farrar, C.R., and N.A. Lieven, "Damage Prognosis: The Future of Structural Health Monitoring," *Philosophical Transactions of the Royal Society A: Mathematical, Physical, and Engineering Sciences*, Vol. 365, 2007, pp. 879–885.

Fröhlich, J., W. Niedermeier, and H.-D. Luginsland, "The Effect of Filler-filler and Filler-elastomer Interaction on Rubber Reinforcement," *Composites Part A: Applied Science and Manufacturing*, Vol. 36, No. 4, 2005, pp. 449–460.

Harms, T., S. Sedigh, and F. Bastianini, "Structural Health Monitoring of Bridges using Wireless Sensor Networks," *Instrumentation & Measurement*, Vol. 13, No. 6, 2010, pp. 14–18.

Hong, H.P., K.H. Jung, N.K. Min, Y.H. Rhee, and C.W. Park, "A Highly Fast Capacitive-type Humidity Sensor using Percolating Carbon Nanotube Films as a Porous Electrode Material, *2012 IEEE Sensors*, 2012, pp. 1–4.

Hu, Y., W.S. Rieutort-Louis, J. Sanz-Robinson, L. Huang, B. Glisic, J.C. Sturm, S. Wagner, and N. Verma, "Large-scale Sensing System Combining Large-area Electronics and CMOS ICs for Structural-health Monitoring," *IEEE Journal of Solid-State Circuits*, Vol. 49, No. 2, 2014, pp. 513–523.

Kang, I., M.J. Schulz, J.H. Kim, V. Shanov, and D. Shi, "A Carbon Nanotube Strain Sensor for Structural Health Monitoring," *Smart Materials and Structures*, Vol. 15, No. 3, 2006.

Kollosche, M., H. Stoyanov, S. Laflamme, and G. Kofod, "Strongly Enhanced Sensitivity in Elastic Capacitive Strain Sensors," *Journal of Materials Chemistry*, Vol. 21, No. 23, 2011, pp. 8292–8294.

Kharroub, S., S. Laflamme, C. Song, D. Qiao, B. Phares, and J. Li, "Smart Sensing Skin for Detection and Localization of Fatigue Cracks," *Smart Materials and Structures*, Vol. 24, No. 6, 2015.

Kugler, H.P., R.G. Stacer, and C. Steimle, "Direct Measurement of Poisson's Ratio in Elastomers," *Rubber Chemistry and Technology*, Vol. 63, No. 4, 1990, pp. 473–487.

Laflamme, S., F. Ubertini, H. Saleem, A. D'Alessandro, A. Downey, H. Ceylan, and A.L. Materazzi, "Dynamic Characterization of a Soft Elastomeric Capacitor for Structural Health Monitoring," *Journal of Structural Engineering*, Vol. 141, No. 8, 2015.

Laflamme, L., M. Kollosche, J.J. Connor, and G. Kofod, "Robust Flexible Capacitive Surface Sensor for Structural Health Monitoring Applications," *Journal of Engineering Mechanics*, Vol. 139, No. 7, 2013a, pp. 879–885.

Laflamme, S., H. Saleem, B. Vasan, R. Geiger, D. Chen, M. Kessler, and K. Rajan, "Soft Elastomeric Capacitor Network for Strain Sensing over Large Surfaces," *IEEE/ASME Transactions on Mechatronics*, Vol. 18, No. 6, 2013b, pp. 1647–1654.

Lipomi, D.J., M. Vosgueritchian, B.C.K. Tee, S.L. Hellstrom, J.A. Lee, C.H. Fox, and Z. Bao, "Skin-like Pressure and Strain Sensors Based on Transparent Elastic Films of Carbon Nanotubes," *Nature Nanotechnology*, Vol. 6, No. 12, 2011, pp. 788–792.

Loh, K.J., T.-C. Hou, J.P. Lynch, and N.A. Kotov, "Carbon Nanotube Sensing Skins for Spatial Strain and Impact Damage Identification," *Journal of Nondestructive Evaluation*, Vol. 28, No. 1, 2009, pp. 9–25.

Pritz, T., "The Poisson's Loss Factor of Solid Viscoelastic Materials," *Journal of Sound and Vibration*, Vol. 306, Nos. 3–5, 2007, pp. 790–802.

Srivastava, R.K., V.S.M. Vemuru, Y. Zeng, R. Vajtai, S. Nagarajaiah, P.M. Ajayan, and A. Srivastava, "The Strain Sensing and Thermal-mechanical Behavior of Flexible Multi-walled Carbon Nanotube/Polystyrene Composite Films," *Carbon*, Vol. 49, No. 12, 2011, pp. 3928–3936.

Stoyanov, H., M. Kollosche, D.N. McCarthy, and G. Kofod, "Molecular Composites with Enhanced Energy Density for Electroactive Polymers," *Journal of Material Chemistry*, Vol. 20, 2010, pp. 7558–7564.

Suster, M., J. Guo, N. Chaimanonart, W. Ko, and D. Young, "A High-performance MEMS Capacitive Strain Sensing System," *Journal of Microelectromechanical Systems*, Vol. 15, No. 5, 2006, pp. 1069–1077.

Tschoegl, N., W. Knauss, and I. Emri, "Poisson's Ratio in Linear Viscoelasticity—A Critical Review," *Mechanics of Time-Dependent Materials*, Vol. 6, No. 1, 2002, pp. 3–51.

Tung, S., Y. Yao, and B. Glisic, "Sensing Sheet: The Sensitivity of Thin-film Full-bridge Strain Sensors for Crack Detection and Characterization," *Measurement Science and Technology*, Vol. 25, No. 7, 2014.

Ubertini, F., S. Laflamme, H. Ceylan, A.L. Materazzi, G. Cerni, H. Saleem, A. D'Alessandro, and A. Corradini, "Novel Nanocomposite Technologies for Dynamic Monitoring of Structures: A Comparison Between Cement-based Embeddable and Soft Elastomeric Surface Sensors," *Smart Materials and Structures*, Vol. 23, No. 4, 2014.

Wada, Y., R. Ito, and H. Ochiai, "Comparison Between Mechanical Relaxations Associated with Volume and Shear Deformations in Styrene-butadiene Rubber," *Journal of the Physical Society of Japan*, Vol. 17, No. 1, 1962, pp. 213–218.

Wilkinson, A., M. Clemens, and V. Harding, "The Effects of SEBS-*g*-maleic Anhydride Reaction on the Morphology and Properties of Polypropylene/PA6/SEBS Ternary Blends," *Polymer*, Vol. 45, No. 15, 2004, pp. 5239–5249.

Wu, J., C. Song, H.S. Saleem, A. Downey, and S. Laflamme, "Network of Flexible Capacitive Strain Gauges for the Reconstruction of Surface Strain, *Measurement Science and Technology*, Vol. 26, No. 5, 2015.